Photocatalysts

DOI: 10.1002/anie.201101969

A Highly Active Titanium Dioxide Based Visible-Light Photocatalyst with Nonmetal Doping and Plasmonic Metal Decoration**

*Qiao Zhang, Diana Q. Lima, Ilkeun Lee, Francisco Zaera, Miaofang Chi, and Yadong Yin**

Since the discovery of its photocatalytic activity under UV light, TiO_2 has been widely studied as a photocatalyst in applications such as water splitting and purification.[1] As pristine TiO_2 only absorbs UV light, much effort has been devoted to developing visible-light-active TiO_2 photocatalysts that can make use of both UV and visible radiation. Many strategies, including metal-ion[2] and nonmetal doping,[3] have been proposed to extend the absorption of TiO_2 to the visible spectrum, but, to date, new materials have typically suffered from low doping concentration and/or low stability against photocorrosion.[3d,4] Noble-metal nanoparticles such as Au and Ag have also been used to enhance the activity of photocatalysts in visible light because of their plasmonic properties.[5] In any case, an improved absorption of photons may not necessarily guarantee significantly better photocatalytic performance because the efficiency of a photocatalyst is also determined by charge separation and transport. As most excited charges may recombine and quench before reaching the surface, small grain size and high crystallinity would be desirable for enhancing charge-separation efficiency that would result in a reduced migration distance of charges and, consequently, in a lower recombination rate.[6] Additionally, metal decoration has also been shown to enhance charge separation in TiO_2 photocatalysts by serving as an electron reservoir.[7] It is therefore expected that a composite of small doped TiO_2 nanocrystals decorated with metal nanoparticles may be a powerful photocatalyst, as all the features discussed above are combined. However, the incompatibility between the synthesis, doping, and decoration procedures means that the production of such nanocomposites has remained a great challenge.

We report herein the design and synthesis, by combining simple sol–gel and calcination processes, of a highly efficient, stable, and cost-effective TiO_2-based photocatalyst with the desired properties mentioned above. The new catalyst has a sandwich structure that comprises a SiO_2 core, a layer of gold nanoparticles (AuNPs), and a doped TiO_2 nanocrystalline shell. The sol–gel process allows for the convenient incorporation of AuNPs into the catalyst with controlled loading and location. TiO_2 is doped with both N and C using an unconventional method that involves introducing 3-aminopropyl-triethoxysilane (APTES), which originally acts as a ligand for immobilization of AuNPs on the surface of the SiO_2 support, but upon subsequent decomposition at high temperature serves as a source of both N and C for doping. Compared to traditional Au/TiO_2 composites, in which AuNPs are loosely attached to the surface of TiO_2 such that they are unstable during calcination and subsequent photocatalysis, the sandwich structures with the AuNPs embedded inside a TiO_2 matrix protects the former from moving together and coagulating.[8] The encapsulation also increases the contact area between the AuNPs and the TiO_2 matrix, and therefore allows for more efficient electron transfer. A third advantage of our nanoarchitecture is that the precontact of Au with a TiO_2 surface can significantly increase the N loading by stabilizing the doped N inside the oxide, and the doped N in turn can enhance the adhesion of AuNPs on the oxide surface through an electron transfer process.[9] As discussed later, only a relatively small quantity (ca. 0.1 wt%) of AuNPs are required for optimal catalytic performance, thus making this catalyst feasible for large-scale practical applications. Herein we demonstrate the excellent performance of the new photocatalysts in degradation reactions of a number of organic compounds under UV, visible light, and direct sunlight.

The fabrication of the sandwich structures is depicted in Figure 1a. SiO_2 particles with a diameter of approximately 400 nm were first synthesized through the Stöber method,[10] then surface-modified with a monolayer of the coupling agent APTES by heating the mixture in isopropanol at 80°C. Citrate-stabilized AuNPs could then be adsorbed onto the silica surface by a strong chemical affinity towards primary amines, as confirmed by the color change of the original Au suspension from red to colorless after extraction by APTES-modified SiO_2 spheres. In the presence of hydroxypropyl cellulose (HPC), the Au/SiO_2 composite colloids were overcoated with a layer of amorphous TiO_2 by hydrolyzing tetrabutyl orthotitanate (TBOT) in ethanol solution.[6a,11]

[*] Q. Zhang, D. Q. Lima, Dr. I. Lee, Prof. F. Zaera, Prof. Y. Yin
Department of Chemistry, University of California
Riverside, CA 92521 (USA)
Fax: (+1) 951-827-4713
E-mail: yadong.yin@ucr.edu
Homepage: http://faculty.ucr.edu/~yadongy/
Dr. M. Chi
Materials Science Division, Oak Ridge National Laboratory
Oak Ridge, TN 37830 (USA)

[**] Financial support of this work was provided by the U.S. Department of Energy (DE-SC0002247). Y.Y. also thanks the Research Corporation for Science Advancement for the Cottrell Scholar Award, 3M for the Nontenured Faculty Grant, and DuPont for the Young Professor Grant. We thank the Central Facility for Advanced Microscopy and Microanalysis at UCR for access to TEM and SEM analysis. Part of the TEM work was performed at the SHaRE user facility at ORNL, which is supported by DOE-BES. The Brazilian National Council for Scientific and Technological Development (CNPq) (grant 202146/2008-1) supported the academic stay of D.Q.L. at University of California in Riverside to carry out part of her experimental work for her PhD thesis in chemistry (UFMG, Brazil).

Supporting information for this article is available on the WWW under http://dx.doi.org/10.1002/anie.201101969.

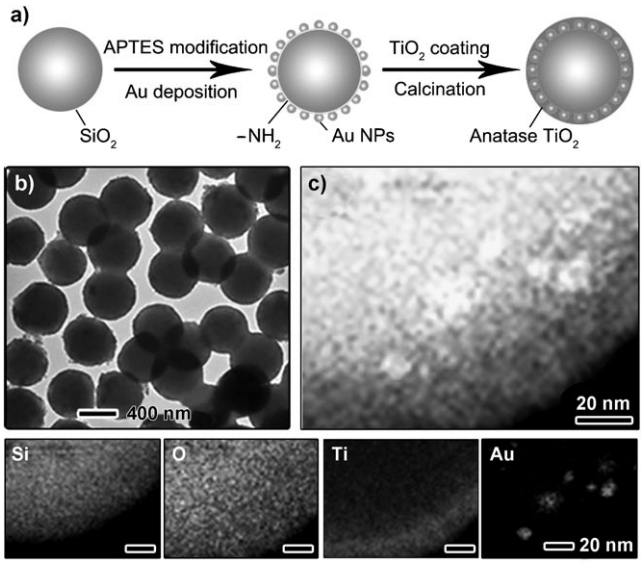

Figure 1. a) Schematic illustration of the fabrication process of the sandwich-structured $SiO_2/Au/TiO_2$ photocatalyst. b) Typical TEM image of the composite photocatalyst. c) Elemental mapping of a single particle with the distribution of individual elements shown in the bottom row.

The reddish composite was finally calcined at 500 °C for 2 h under ambient conditions to produce a blue powder consisting of uniform spheres with an average diameter of approximately 430 nm, as shown in the transmission electron microscopy (TEM) image in Figure 1 b. Energy dispersive X-ray (EDX) elemental mapping of a single sphere (Figure 1 c) clearly confirms the expected sandwich structure. Observation by TEM at higher magnification reveals that the outer TiO_2 shell is composed of small nanoparticle grains with sizes of 8–15 nm, which are optimal for anatase photocatalysts.[6a,12] Nitrogen adsorption–desorption isotherm measurements on this sample suggest an average BET surface area of approximately 45.1 $m^2 g^{-1}$, thus confirming the porous nature of the TiO_2 shell.

Figure 2 shows X-ray diffraction (XRD) data used to identify the crystallographic phases of the titania in the as-prepared sandwich-structured catalysts, along with two reference samples including commercial anatase TiO_2 powder and P25 aeroxide. As shown in Figure 2 a, the sandwich structures show all the characteristic diffraction peaks also found in commercial anatase TiO_2, with cell parameters $a = b = 3.78$ Å, $c = 9.51$ Å (JCPDS card no. 73-1764). The peak broadening of the sandwich structures suggests that the shells are composed of small nanocrystalline grains, as is consistent with our TEM observation. No characteristic peaks of crystallized gold can be found in our sample because of its very low concentration. As expected, P25 was found to be a mixture of anatase and rutile phases.[6a]

Diffuse reflectance UV/Vis spectroscopy was used to study the optical properties of the sandwich-structured photocatalyst and contrast those with the reference samples (Figure 2 b). While the commercial anatase sample strongly absorbs light only in the UV region, noticeable absorption in the visible region can be observed for all $SiO_2/APTES/TiO_2$ structures, even in the absence of AuNPs. This result confirms

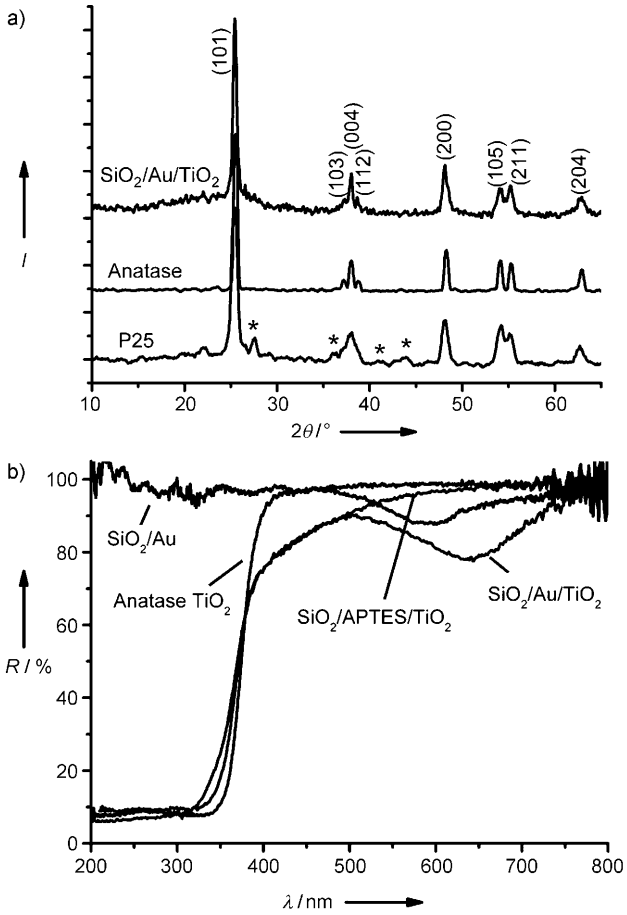

Figure 2. a) XRD patterns of the $SiO_2/Au/TiO_2$ photocatalyst, commercial anatase TiO_2 and P25 aeroxide. * denotes rutile phase TiO_2. b) UV/Vis diffuse reflectance spectra of the three TiO_2-based photocatalysts and a control sample of AuNP-decorated silica particles.

doping of TiO_2 with N and/or C as reported by Sato, and Giamello and co-workers.[13] Moreover, with AuNPs, another absorption band at around 650 nm appears, which can be mainly ascribed to the surface plasmon resonance of AuNPs. Compared to a reference sample consisting of AuNP-decorated SiO_2 spheres, which shows an absorption band at around 590 nm, the new absorption band in the $SiO_2/APTES/Au/TiO_2$ structure (simply denoted as $SiO_2/Au/TiO_2$ in later discussions) is red-shifted by approximately 60 nm, a difference that can be attributed to the high refractive index of the TiO_2 ($n = 2.488$ for pure anatase TiO_2) that surrounds the AuNPs.[5c] This result also suggests a good contact between AuNPs and TiO_2 grains.

X-ray photoelectron spectroscopy (XPS) was used to investigate the C and/or N doping in the TiO_2 shells. Without doping, for the simple TiO_2-coated SiO_2 sample, Ti exhibits a $2p_{3/2}$ peak at 458.5 eV, which corresponds to the binding energy of Ti^{4+} in TiO_2 (Figure 3 a).[14] Once APTES is introduced between the SiO_2 core and the TiO_2 shell, however, the Ti 2p peak shifts to a lower binding energy of 458.2 eV. This shift is indicative of the incorporation of N and/or C into the TiO_2 lattice.[15] The low loadings used and the TiO_2 overcoating result in relatively weak XPS signals for N and C, thus making it difficult to identify the exact nature of

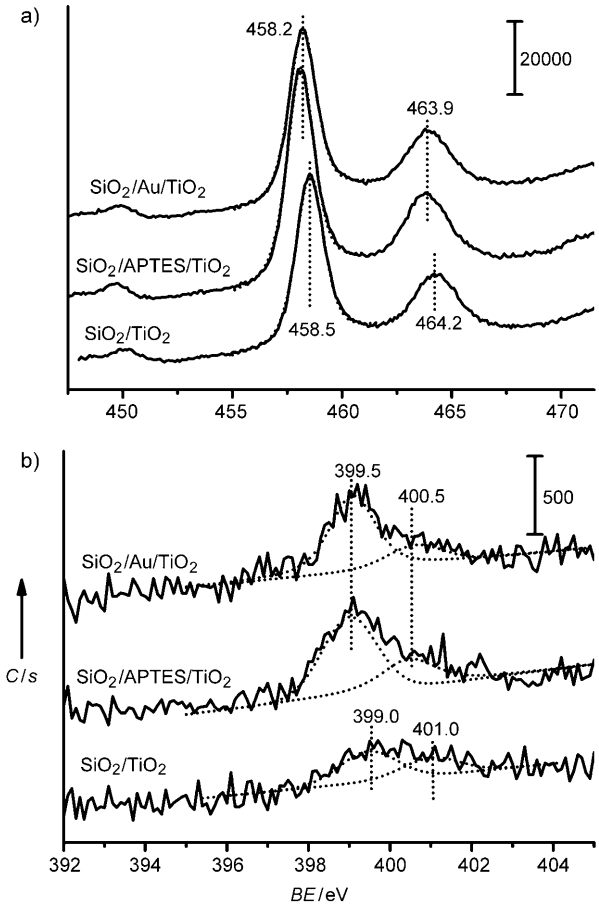

Figure 3. XPS measurements for the as-obtained $SiO_2/Au/TiO_2$ photocatalyst: a) Ti 2p, and b) N 1s. All the XPS data have been calibrated with the binding energy of Si–O from SiO_2 at 103.4 eV.

the doped species. As shown in Figure 3b, all the samples display a weak and broad N 1s XPS peak around 400.5–401.0 eV, which can be attributed to adsorbed N_2 molecules.[16] The N 1s XPS data of nitrogen-doped TiO_2 have recently been reported to exhibit a peak at 396 eV,[16–17] which arises from the substitutionally doped N^{3-} component of Ti–N, but we could not detect any signal at this position with our SiO_2/APTES/TiO_2 and SiO_2/Au/TiO_2 samples, probably because of the limited doping at the vicinity of SiO_2/TiO_2 interface. Instead, we observed a peak at 399.0 eV which may be produced by jointly bonded C–N in $TiO_{2-x-y}N_xC_y$ films.[18] The existence of additional C resulting from the decomposition of APTES has also been confirmed by the C 1s spectra (see the Supporting Information).[18–19]

The photocatalytic activity was evaluated by monitoring its characteristic absorption band at 553 nm to measure the degradation rate of rhodamine B (RhB) under light irradiation. Unlike many previous reports in which the incorporation of a metal into TiO_2 degrades catalytic performance in the UV region,[20] the sandwiched structures show performance comparable to P25 under UV irradiation, thus attesting to the overall positive impact of the nonmetal doping and gold decoration on the catalytic activity. Moreover, under visible light irradiation ($\lambda > 400$ nm), the SiO_2/Au/TiO_2 nanostructures display significantly higher efficiency than that of P25. As shown in Figure 4a, the sandwich-structured photocatalyst can decompose approximately 96% of RhB in 5 h, while P25 containing an equivalent amount of TiO_2 can convert only about 42% of RhB under identical conditions. Commercial anatase is essentially inactive.

To investigate the origin of the enhanced photocatalytic activity, we also compared the performance of the SiO_2/Au/TiO_2 photocatalyst to SiO_2/TiO_2 and SiO_2/APTES/TiO_2 composites synthesized under similar conditions by using silica cores of the same size and TiO_2 shells of the same thickness. Before catalysis, the TiO_2 in all samples was identified as pure anatase by XRD. As shown in Figure 4a, without the modification of APTES, the SiO_2/TiO_2 core–shell structures show very low activity under visible light irradiation. However, after C/N doping, the core–shell photocatalyst becomes active and shows 48% degradation of RhB in 5 h. This is already an improvement over the widely recognized P25 aeroxide photocatalyst, which shows considerable visible-light activity because of the presence of rutile phase.[21] Additional decoration of the SiO_2/TiO_2 interface with 0.1% of AuNPs further doubles the decomposition rate.

Chronoamperometry (CA) measurements were performed to characterize the photogenerated current density under a potential of 0.8 V and periodic illumination of visible light ($\lambda > 400$ nm). As indicated in Figure 4b, photogenerated currents were seen for all samples, but SiO_2/Au/TiO_2 showed a significantly higher value (ca. 0.80 $\mu A\,cm^{-2}$) than P25 (ca. 0.45 $\mu A\,cm^{-2}$) and SiO_2/APTES/TiO_2 (ca. 0.40 $\mu A\,cm^{-2}$). The shape of the CA curves is well maintained after many cycles of light illumination, thus implying very good photocatalytic stability.

It is clear that decoration of titania-based photocatalysts with AuNPs is an important factor to achieve the high catalytic efficiency. A systematic study was carried out to assess this effect by varying the loading of AuNPs from 0 to 0.5 wt% in six otherwise identical samples (Figure 4c). Interestingly, the visible-light activity of the samples peaks at 0.1 wt% loading of AuNPs. It is generally understood that AuNPs supported on TiO_2 have three probable functions in photocatalysis: 1) to help harvest the visible-light energy by their plasmonic properties,[5c] 2) to enhance charge separation by serving as an electron reservoir,[7,22] and 3) to act as a recombination center, which negatively affects catalytic activity.[23] When the loading of AuNPs is low, their primary function is to enhance the charge separation and hence promote the oxidation of organic molecules under visible light. However, excessive amounts of metal particles may also deteriorate the catalytic performance by increasing the occurrence of exciton recombination,[23] with the reaction rate gradually decreasing when the loading of AuNPs exceeds 0.1 wt%. The low loading (0.1 wt%) of the AuNPs required for achieving high catalytic performance also has practical significance in terms of cost: many prior reports on Au/TiO_2 composite photocatalysts require Au loading of approximately 1–5 wt%, which has prevented their large-scale application.[22b]

In addition to the effects on light harvesting and charge separation, the AuNPs may also contribute to the enhancement in nonmetal doping for TiO_2. Sanz and co-workers have

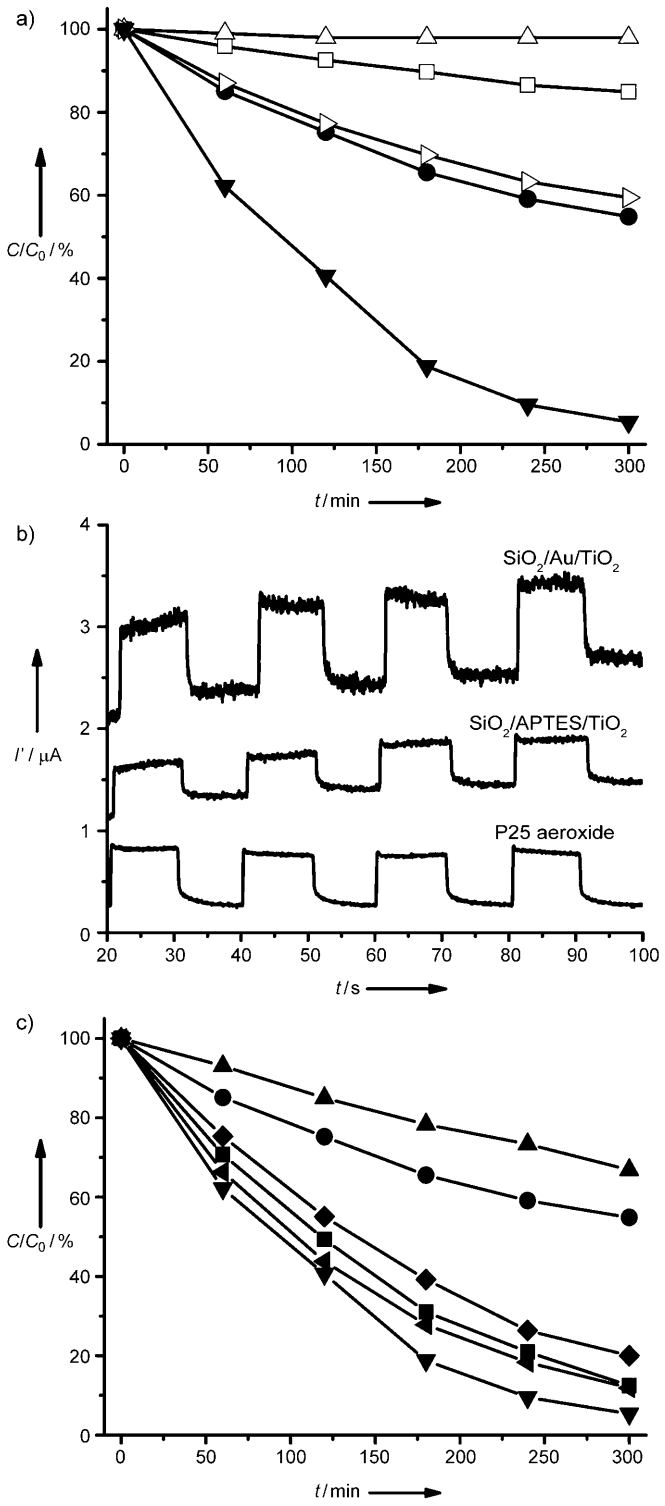

Figure 4. a) Photodegradation of RhB by using commercial anatase TiO_2 (△), SiO_2/TiO_2 (□), P25 aeroxide (▷), $SiO_2/APTES/TiO_2$ (●), and $SiO_2/Au(0.1\%)/TiO_2$ (▼) as photocatalysts under visible-light illumination ($\lambda > 400$ nm). b) Chronoamperometry measurements of P25, $SiO_2/APTES/TiO_2$, and $SiO_2/Au/TiO_2$ under periodic illumination with visible light. c) Influence of AuNP loading (● 0.00, ◆ 0.05, ▼ 0.10, ◀ 0.20, ■ 0.30, ▲ 0.50% Au) on the catalytic activity of $SiO_2/Au/TiO_2$ sandwich structures studied by using the decomposition of RhB as the model system.

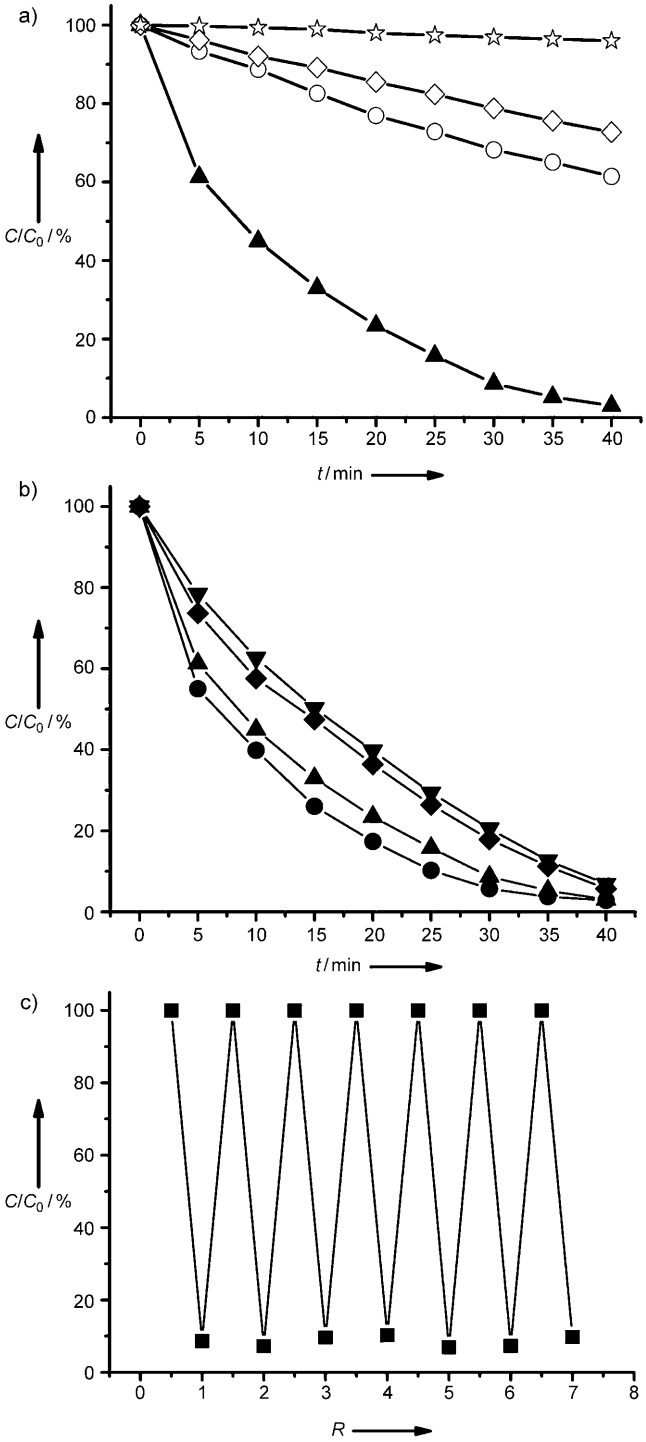

Figure 5. a) Photodegradation of RhB without catalyst (*) and with anatase TiO_2 (◇), P25 (○), and $SiO_2/Au/TiO_2$ (▲) as the photocatalysts under direct sunlight illumination. b) Photodegradation of RhB (▲), R6G (▼), methylene blue (●), and 2,4-dichlorophenol (◆) with $SiO_2/Au/TiO_2$ sandwich-structured catalyst under direct sunlight illumination. c) Seven cycles of the photodegradation of RhB with $SiO_2/Au/TiO_2$ photocatalyst under sunlight illumination. The duration of sunlight exposure in each cycle is 30 min.

demonstrated both theoretically and experimentally that Au preadsorption on TiO_2 surfaces can significantly stabilize implanted N, increase the reachable amount of N loading in the oxide, and enhance Au surface adhesion energy by electron transfer from the Au 6s orbitals to the partially occupied N 2p orbitals.[9] As the nonmetal doping process usually requires annealing at elevated temperatures, which may cause the AuNPs to sinter, the unique sandwich structure proposed in this work represents an ideal system to overcome sintering: AuNPs are unable to move within the TiO_2 matrix, and thus coagulation during calcination is prevented, high stability is ensured, and Au/TiO_2 surface contact is improved.

To explore the photocatalytic activity of our samples for real applications, the photodegradation of organic compounds was investigated under natural sunshine, which contains both UV, visible, and IR light. As shown in Figure 5a, sunlight can completely decompose RhB molecules within 40 min with the aid of sandwich-structured photocatalysts, while the conversion only reaches approximate values of 38% with P25 and 27% with the commercial anatase sample during the same period. We also tested the $SiO_2/Au/TiO_2$-catalyzed degradation of other organic molecules under sunlight, including rhodamine 6G (R6G), methylene blue (MB), and 2,4-dichlorophenol (2,4-DCP) at the same initial concentration. As shown in Figure 5b, all of those molecules can be decomposed almost completely ($>93\%$) within 40 min. As shown in Figure 5c, these photocatalysts are also mechanically robust and chemically stable: they can be recovered and reused to catalyze multiple cycles of degradation reactions under direct sunlight.

In summary, we have demonstrated a sandwich-structured $SiO_2/Au/TiO_2$ photocatalyst that shows high efficiency in catalyzing decomposition of organic compounds under illumination of UV, visible light, and natural sunlight. The structural design of the photocatalyst takes advantage of the synergetic interaction between adsorbed gold and implanted nitrogen, and produces stable nonmetal-doped anatase nanoparticles with precisely controlled AuNPs decoration. The excellent photocatalytic efficiency can be attributed to the interfacial nonmetal doping, which improves visible light activity, to the plasmonic metal decoration, which enhances light harvesting and charge separation, and to the small grain size of anatase nanocrystals, which reduces the exciton recombination rate.

Received: March 20, 2011
Revised: May 19, 2011
Published online: June 24, 2011

Keywords: doping · nanoparticles · photocatalysts · plasmonic metals · titanium dioxide

[1] a) A. Fujishima, K. Honda, *Nature* **1972**, *238*, 37–38; b) B. O'Regan, M. Gratzel, *Nature* **1991**, *353*, 737–740.
[2] W. Y. Choi, A. Termin, M. R. Hoffmann, *J. Phys. Chem.* **1994**, *98*, 13669–13679.
[3] a) R. Asahi, T. Morikawa, T. Ohwaki, K. Aoki, Y. Taga, *Science* **2001**, *293*, 269–271; b) S. Sakthivel, H. Kisch, *Angew. Chem.* **2003**, *115*, 5057–5060; *Angew. Chem. Int. Ed.* **2003**, *42*, 4908–4911; c) S. U. M. Khan, M. Al-Shahry, W. B. Ingler, *Science* **2002**, *297*, 2243–2245; d) A. Emeline, V. Kuznetsov, V. Rybchuk, N. Serpone, *Int. J. Photoenergy* **2008**, *2008*, 1–19; e) X. Chen, L. Liu, P. Y. Yu, S. S. Mao, *Science* **2011**, *331*, 746–750.
[4] a) J. Graciani, L. J. Alvarez, J. A. Rodriguez, J. F. Sanz, *J. Phys. Chem. C* **2008**, *112*, 2624–2631; b) M. Batzill, E. H. Morales, U. Diebold, *Phys. Rev. Lett.* **2006**, *96*, 026103; c) A. Nambu, J. Graciani, J. A. Rodriguez, Q. Wu, E. Fujita, J. F. Sanz, *J. Chem. Phys.* **2006**, *125*, 094706.
[5] a) A. Furube, L. Du, K. Hara, R. Katoh, M. Tachiya, *J. Am. Chem. Soc.* **2007**, *129*, 14852–14853; b) S. Naya, A. Inoue, H. Tada, *J. Am. Chem. Soc.* **2010**, *132*, 6292–6293; c) K. Awazu, M. Fujimaki, C. Rockstuhl, J. Tominaga, H. Murakami, Y. Ohki, N. Yoshida, T. Watanabe, *J. Am. Chem. Soc.* **2008**, *130*, 1676–1680.
[6] a) M. Ye, Q. Zhang, Y. Hu, J. Ge, Z. Lu, L. He, Z. Chen, Y. Yin, *Chem. Eur. J.* **2010**, *16*, 6243–6250; b) Q. Zhang, J.-B. Joo, Z. Lu, M. Dahl, D. Oliveira, M. Ye, Y. Yin, *Nano Res.* **2011**, *4*, 103–114.
[7] J. Li, H. C. Zeng, *Chem. Mater.* **2006**, *18*, 4270–4277.
[8] a) Q. Zhang, I. Lee, J. Ge, F. Zaera, Y. Yin, *Adv. Funct. Mater.* **2010**, *20*, 2201–2214; b) J. Ge, Q. Zhang, T. Zhang, Y. Yin, *Angew. Chem.* **2008**, *120*, 9056–9060; *Angew. Chem. Int. Ed.* **2008**, *47*, 8924–8928; c) I. Lee, Q. Zhang, J. Ge, Y. Yin, F. Zaera, *Nano Res.* **2011**, *4*, 115–123.
[9] J. Graciani, A. Nambu, J. Evans, J. A. Rodriguez, J. F. Sanz, *J. Am. Chem. Soc.* **2008**, *130*, 12056–12063.
[10] W. Stober, A. Fink, E. Bohn, *J. Colloid Interface Sci.* **1968**, *26*, 62–69.
[11] a) J. W. Lee, M. R. Othman, Y. Eom, T. G. Lee, W. S. Kim, J. Kim, *Microporous Mesoporous Mater.* **2008**, *116*, 561–568; b) M. Ye, S. Zorba, L. He, Y. Hu, R. T. Maxwell, C. Farah, Q. Zhang, Y. Yin, *J. Mater. Chem.* **2010**, *20*, 7965–7969.
[12] a) M. Anpo, T. Shima, S. Kodama, Y. Kubokawa, *J. Phys. Chem.* **1987**, *91*, 4305; b) S. Y. Chae, M. K. Park, S. K. Lee, T. Y. Kim, S. K. Kim, W. I. Lee, *Chem. Mater.* **2003**, *15*, 3326; c) C.-C. Wang, Z. Zhang, J. Y. Ying, *Nanostruct. Mater.* **1997**, *9*, 583.
[13] a) S. Sato, *Chem. Phys. Lett.* **1986**, *123*, 126–128; b) S. Livraghi, M. C. Paganini, E. Giamello, A. Selloni, C. Di Valentin, G. Pacchioni, *J. Am. Chem. Soc.* **2006**, *128*, 15666–15671.
[14] U. Diebold, T. Madey, *Surf. Sci. Spectra* **1996**, *4*, 227–231.
[15] J. Wang, D. N. Tafen, J. P. Lewis, Z. L. Hong, A. Manivannan, M. J. Zhi, M. Li, N. Q. Wu, *J. Am. Chem. Soc.* **2009**, *131*, 12290–12297.
[16] N. C. Saha, H. G. Tompkins, *J. Appl. Phys.* **1992**, *72*, 3072–3079.
[17] a) H. Irie, Y. Watanabe, K. Hashimoto, *J. Phys. Chem. B* **2003**, *107*, 5483–5486; b) T. Sano, N. Negishi, K. Koike, K. Takeuchi, S. Matsuzawa, *J. Mater. Chem.* **2004**, *14*, 380–384; c) O. Diwald, T. L. Thompson, T. Zubkov, E. G. Goralski, S. D. Walck, J. T. Yates, *J. Phys. Chem. B* **2004**, *108*, 6004–6008.
[18] J. Yang, H. Z. Bai, X. C. Tan, J. S. Lian, *Appl. Surf. Sci.* **2006**, *253*, 1988–1994.
[19] a) K. R. Wu, C. H. Hung, *Appl. Surf. Sci.* **2009**, *256*, 1595–1603; b) H. Kamisaka, T. Adachi, K. Yamashita, *J. Chem. Phys.* **2005**, *123*, 084704; c) G. Iucci, M. Dettin, C. Battocchio, R. Gambaretto, C. Di Bello, G. Polzonett, *Mater. Sci. Eng. C* **2007**, *27*, 1201–1206; d) W. J. Ren, Z. H. Ai, F. L. Jia, L. Z. Zhang, X. X. Fan, Z. G. Zou, *Appl. Catal. B* **2007**, *69*, 138–144; e) Q. Xiao, J. Zhang, C. Xiao, Z. C. Si, X. O. Tan, *Solar Energy* **2008**, *82*, 706–713.
[20] Z. Liu, W. Hou, P. Pavaskar, M. Aykol, S. B. Cronin, *Nano Lett.* **2011**, *11*, 1111–1116.
[21] D. C. Hurum, A. G. Agrios, K. A. Gray, T. Rajh, M. C. Thurnauer, *J. Phys. Chem. B* **2003**, *107*, 4545–4549.
[22] a) V. Subramanian, E. E. Wolf, P. V. Kamat, *J. Am. Chem. Soc.* **2004**, *126*, 4943–4950; b) A. Primo, A. Corma, H. Garcia, *Phys. Chem. Chem. Phys.* **2011**, *13*, 886–910.
[23] Y. M. Wu, H. B. Liti, J. L. Zhang, F. Chen, *J. Phys. Chem. C* **2009**, *113*, 14689–14695.

